



Contents lists available at ScienceDirect

Quaternary Science Reviews

journal homepage: www.elsevier.com/locate/quascirev

Holocene glacier and deep water dynamics, Adélie Land region, East Antarctica

Delphine Denis^{a,*}, Xavier Crosta^a, Sabine Schmidt^a, Damien S. Carson^b, Raja S. Ganeshram^b, Hans Renssen^c, Viviane Bout-Roumazeilles^d, Sebastien Zaragosi^a, Bernard Martin^a, Michel Cremer^a, Jacques Giraudeau^a

^aEPOC, UMR 5805 CNRS, Université Bordeaux 1, Avenue des Facultés, F-33405 Talence Cedex, France

^bSchool of GeoSciences, The University of Edinburgh, Grant Institute, West Mains Road, Edinburgh EH9 3JW, UK

^cFaculty of Earth and Life Sciences, Vrije Universiteit Amsterdam, De Boelelaan 1085, NL-1081 HV Amsterdam, The Netherlands

^dFRE 2255 Sédimentologie & Géodynamique, Université des Sciences et Technologies de Lille 1, F-59655 Villeneuve d'Ascq, France

ARTICLE INFO

Article history:

Received 21 March 2008

Received in revised form

10 December 2008

Accepted 30 December 2008

Available online xxx

ABSTRACT

This study presents a high-resolution multi-proxy investigation of sediment core MD03-2601 and documents major glacier oscillations and deep water activity during the Holocene in the Adélie Land region, East Antarctica. A comparison with surface ocean conditions reveals synchronous changes of glaciers, sea ice and deep water formation at Milankovitch and sub-Milankovitch time scales. We report (1) a deglaciation of the Adélie Land continental shelf from 11 to 8.5 cal ka BP, which occurred in two phases of effective glacier grounding-line retreat at 10.6 and 9 cal ka BP, associated with active deep water formation; (2) a rapid glacier and sea ice readvance centred around 7.7 cal ka BP; and (3) five rapid expansions of the glacier–sea ice systems, during the Mid to Late Holocene, associated to a long-term increase of deep water formation. At Milankovitch time scales, we show that the precessionnal component of insolation at high and low latitudes explains the major trend of the glacier–sea ice–ocean system throughout the Holocene, in the Adélie Land region. In addition, the orbitally-forced seasonality seems to control the coastal deep water formation via the sea ice–ocean coupling, which could lead to opposite patterns between north and south high latitudes during the Mid to Late Holocene. At sub-Milankovitch time scales, there are eight events of glacier–sea ice retreat and expansion that occurred during atmospheric cooling events over East Antarctica. Comparisons of our results with other peri-Antarctic records and model simulations from high southern latitudes may suggest that our interpretation on glacier–sea ice–ocean interactions and their Holocene evolutions reflect a more global Antarctic Holocene pattern.

© 2009 Elsevier Ltd. All rights reserved.

1. Introduction

The East Antarctic Ice Sheet (EAIS) stores 79% of the global ice volume (Wagner and Melles, 2007), and thus directly influences both Antarctic and global climate, due to its influence on the albedo of the Southern Hemisphere, thermohaline circulation, and atmospheric circulation (Ingólfsson and Hjort, 1999). A better understanding of the impact of glacier systems and the associated climate feedbacks, particularly through the sea ice cycle and the magnitude

of deep water formation (Joughin and Padman, 2003) is important for future climate predictions (DeConto et al., 2007). Glaciers appear to react rapidly to Holocene climatic changes as demonstrated by several glacier advances and retreats documented around Antarctica (Ingólfsson et al., 1998 and references therein) and around the world (Solomina et al., 2008, and references therein). However, these reconstructed glacier movements appear erratic in time and space around Antarctica and lack significant correlation with major changes during the Holocene (Wagner and Melles, 2007) as documented from ice cores (Masson et al., 2000; Masson-Delmotte et al., 2004), continental archives (Ingólfsson et al., 1998), marine sediment cores (Hodell et al., 2001; Nielsen et al., 2004) and model simulations (Renssen et al., 2005a). It is expected that ice sheets, bedrock topography, atmosphere, ocean circulation and sea ice factors determine the timing, the dynamic and the amplitude of glacier fluctuations. There is, however, no clear evidence of the implicated forcing factors and subsequent impacts of glacier movement on other climatic components such as

* Corresponding author. Tel.: +33 5 40 00 84 38; fax: +33 5 56 84 08 48.

E-mail addresses: d.denis@epoc.u-bordeaux1.fr (D. Denis), x.crosta@epoc.u-bordeaux1.fr (X. Crosta), s.schmidt@epoc.u-bordeaux1.fr (S. Schmidt), d.s.carson@sms.ed.ac.uk (D.S. Carson), r.ganeshram@ed.ac.uk (R.S. Ganeshram), hans.rensen@geo.falw.vu.nl (V. Renssen), viviane.bout@univ-lille1.fr (V. Bout-Roumazeilles), s.zaragosi@epoc.u-bordeaux1.fr (S. Zaragosi), b.martin@epoc.u-bordeaux1.fr (Bernard Martin), m.cremer@epoc.u-bordeaux1.fr (M. Cremer), j.giraudeau@epoc.u-bordeaux1.fr (J. Giraudeau).

sea ice and deep water formation. Laminated sediments from Antarctic inner shelf basins, allow sub-seasonal to millennial reconstructions of the Holocene that may improve our understanding of climatic changes that occurred on decadal time scales. The Dumont d'Urville Trough in the Adélie Land region of the East Antarctica Margin (EAM) has received little attention despite evidence of very high sediment accumulation rates (Leventer et al., 2006). Here we present a study on marine sediment core MD03-2601, retrieved from the Dumont d'Urville Trough, located in the Adélie Land margin that contains 40 m of Holocene laminated diatom ooze. Previous data obtained from the same sedimentary archive have shown that in this region, the Holocene can be divided into two different climatic periods: a warm Hypsithermal, interrupted by a cool event, and a colder Neoglacial (Crosta et al., 2007). Based on a multi-proxy approach, this study aims to better understand the interaction of the different climatic sub-systems during the Holocene, with particular focus on episodes of glacier advance and retreat that occurred throughout these different climatic regimes. Holocene movements of glaciers are investigated in parallel to deep water production, and compared with surface ocean conditions (Crosta et al., 2008), modelled sea ice cover, air temperatures and precipitations (Renssen et al., 2005a, this study), and East Antarctic climate (Masson et al., 2000).

2. Adélie Land margin setting

The Dumont d'Urville Trough (DDUT) is located off Adélie Land on the EAM and is oriented SE–NW (Fig. 1A). It is composed of a succession of glacial depressions enclosed between the Dibble Bank to the west, and the Adélie Bank to the East. The Adélie Land region is dissected by several glaciers injecting freshwater and terrigenous particles in the coastal area. The majority of freshwater and terrigenous material comes from the Zélée, Astrolabe and Français glaciers, located 200, 120 and 55 km from the core site respectively (Fig. 1A). The DDUT shows evidences of streamlined elongated ridges, known as mega-scale glacial lineations (Shipp et al., 1999; McMullen et al., 2006) that testify to past ice streaming

(Fig. 1B). Two different ice stream directions are apparent, one perpendicular to the coastal line and in front of the Français glacier, and the other parallel to the coastal line, which probably originates from the Zélée glacier (Fig. 1B).

At present, the coastal area off Adélie Land is exposed to strong katabatic winds (Periard and Pettre, 1993) that support the DDU polynya throughout the winter season (Adolphs and Wendler, 1995; Arrigo and van Dijken, 2003) (Fig. 1A), located southward at 66.11°S, 139.31°E. Considered as ice factories, polynyas partly control the sea ice production. At the present time, sea ice covers the core site for 7–9 months of the year from February/March to November/December (Arrigo and van Dijken, 2003). As katabatic winds are directly induced by topography, we assume that the DDU polynya has been a persistent phenomenon throughout the Holocene period.

The DDUT is influenced by several water masses (Rintoul, 1998; Bindoff et al., 2000a,b; Williams and Bindoff, 2003): (1) the wind-driven East Wind Drift (EWD) also called Antarctic Coastal Current (ACC), which flows westward at the surface; (2) the Antarctic Surface water (AASW) constituting the near-surface layer on the continental shelf that joins up westward the EWD; (3) the Modified Circumpolar Deep Water (MCDW), which upwells at the Antarctic Divergence; and (4) the High Salinity Shelf Water (HSSW), formed by brine-rejection during winter sea ice formation and cooling of the MCDW, which flows northward as part of the Adélie Land Bottom Water (ALBW) (Fig. 1A). ALBW is characterised by cold, relatively fresh waters with high O₂ content that can rest for several years in the depressions of the continental shelf (Rintoul and Bullister, 1999). A CTD profile obtained on the MD03-2601 core site displays the same characteristic as the ALBW (θ : -1.465 °C, S: 34.511 at 721 m water depth). On Adélie Land, significant cross-shelf transport of ALBW is recorded at about 135°E (Beckmann and Pereira, 2003). Westward flow of ALBW indicates that bottom water formation occurs east of 135°E and may originate from Commonwealth Bay and Mertz Glacier Tongue, where large perennial and recurrent polynyas occur (Cavaliere and Martin, 1985; Massom et al., 1998; Rintoul, 1998; Williams and Bindoff, 2003; Arrigo and

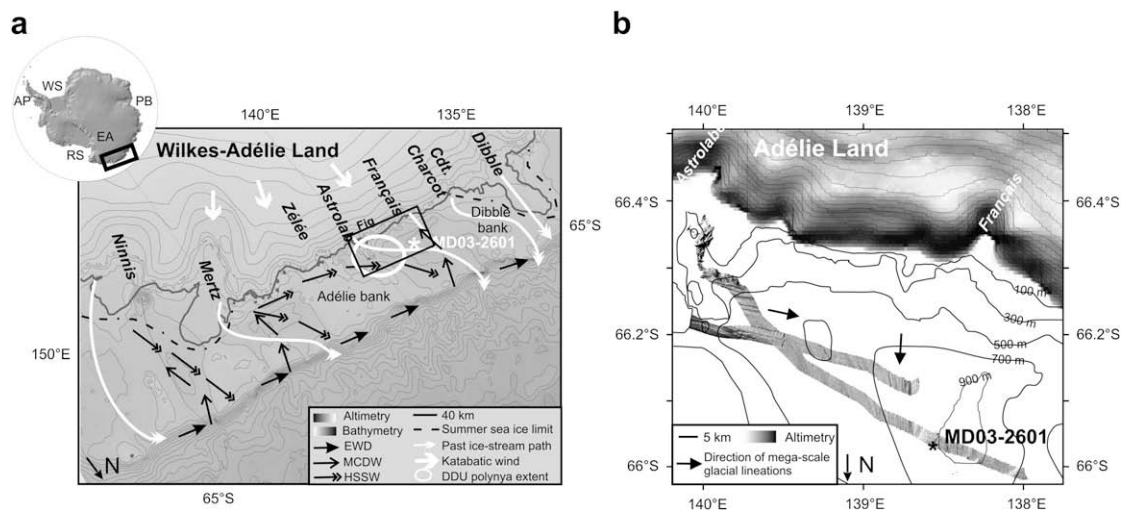


Fig. 1. Map showing the location of sediment core MD03-2601, altimetry and bathymetry in the study area, location of glaciers (in italic). (A) Limit of summer sea-ice cover (Schweitzer, 1995), location of past ice-streams (Massom et al., 1998; Escutia et al., 2003), katabatic wind directions and average winter extent of the DDU polynya (Arrigo and van Dijken, 2003). Winter sea ice covers the whole oceanic area encompassed by the map. EWD, East Wind Drift; MCDW, Modified Circumpolar Deep Water; HSSW, High Salinity Shelf Water; MGT, Mertz Glacier Tongue. The inset narrows the location of the studied area regarding Antarctica, AP, Antarctic Peninsula; WS, Weddell Sea; PB, Prydz Bay; RS, Ross Sea; EA, East Antarctica plateau. (B) Shaded Bathymetric data are provided from the multibeam echosounder (TSM 5265) surveys of the area conducted onboard the R/V *Marion Dufresne II* (IPEV) during the CADO cruise. Note the location of mega-scale lineation, testifying to past ice streaming. Bathymetry data are based on ETOPO02 data set from <http://www.ngdc.noaa.gov/mgg/fliers/01mgg04.html>.

van Dijken, 2003). The Marginal Ice Zone is believed to be macro- and micro-nutrient rich, and ice melting produces a stratified stable environment favourable for diatom blooms (Leventer, 1992).

3. Material and methods

Piston core MD03-2601 (66°03.07'S; 138°33.43'E; 746 m water depth) was recovered from the slope of one of the depressions composing the DDUT in 2003, during MD130 Images X cruise (CADO—Coring Adélie Diatom Oozes) on board R.V. *Marion Dufresne II* (Fig. 1A). The 40 m long sediment core is composed of diatom ooze alternating with structureless greenish ooze and millimetre to centimetre thick green-to-dark seasonal laminations (Denis et al., 2006). Sediment lithology is very fine from clay to silt fraction. The sediment texture is cottony due to the high abundance of diatom frustules. Bioturbation marks are very scarce throughout the core.

3.1. Age model

Ten radiocarbon dates were performed on MD03-2601 at the Leibniz Laboratory, Kiel, Germany. Nine ^{14}C were completed on the humic fraction of bulk organic matter and one ^{14}C was completed on calcite shells and fragments (Crosta et al., 2007). The radiocarbon dates used to construct the age model are the same dates used in Crosta et al. (2007, 2008), e.g. the humic acid dates, with the exception of both 998 and 1498 cm dates, which are incoherent with the meteoritic impact signal, recorded elsewhere at 4 cal ka BP (Courty et al., 2007). Nevertheless, the MD03-2601 age model constructed in this study is different from these previous studies (Fig. 2, Table 1). We calibrated raw ^{14}C dates to calendar ages using Calib 5.0 (Stuiver et al., 2005) and the marine calibration curve Marine04 (Hughen et al., 2004) with a reservoir age of 1300 years as advised for this region (Ingólfsson et al., 1998) (Table 1). Furthermore, we used a linear interpolation between control points, instead of linear regression (Crosta et al., 2007) to conserve changes of sedimentation rates that is necessary to calculate the $^{230}\text{Th}_{\text{xs}}$ (Fig. 2, see Section 3.2.1). It is worth noting that the date based on the calcite shells and fragments of the crinoid pieces presents an age only 400 years younger than surrounding humic dates. This difference highlights the maximum age error within humic acid dates of the age model. MD03-2601 therefore spans the last 11 cal ka BP, with an average sedimentation rate of 0.4 cm yr^{-1} . The first millennium was lost during coring (Fig. 2).

3.2. Rationale for proxy selection

Margin sites of high sediment accumulation are often zones of preferential deposition of redistributed sediment, especially when bottom water circulation is intense (Hall and McCave, 2000; Francois et al., 2004). We used two proxies ($^{230}\text{Th}_{\text{excess}}$, sortable silt) in order to better constrain the sediment redistribution and the bottom water circulation.

3.2.1. $^{230}\text{Th}_{\text{excess}}$

The $^{230}\text{Th}_{\text{excess}}$ excess method estimates the contribution of the lateral sedimentary inputs, named the focusing factor (Francois et al., 2004, and references therein). The ^{230}Th geochemical behaviour permits to calculate an expected flux of scavenged ^{230}Th , which is function of the thickness of the water column and of the radioactive decay law. Indeed, the production rate of ^{230}Th in sea water is constant because it results from the disintegration of ^{234}U , which is nearly constant in the ocean because of its long residence time (Chen et al., 1986). Furthermore, and contrary to its radioactive parent, ^{230}Th presents a strong affinity with the particulate phase and is therefore rapidly scavenged and deposited on the sea floor

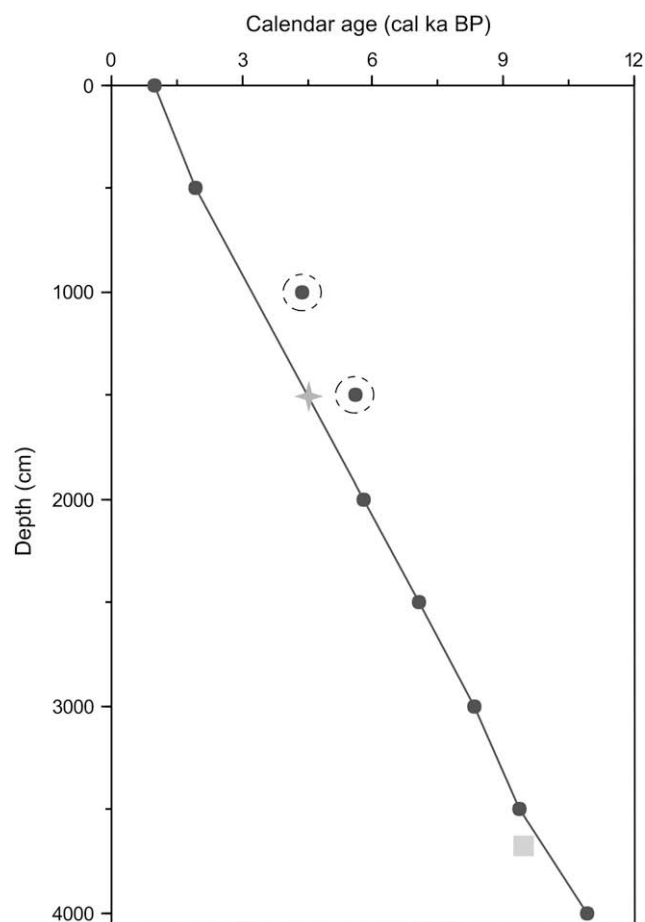


Fig. 2. MD03-2601 age model (black line). ^{14}C dates from humic acid are represented by black point. Two points appear out of the age model possibly because of old carbon input (dashed circles). The grey star represents the depth at which the 4000 yr BP meteoritic impact was evidenced (Courty et al., 2007). ^{14}C date from calcite shells and fragments is symbolised by a grey square. Dating uncertainties at 1σ level are within by the symbol points.

Table 1
Age model of core MD03-2601.

Depth cm bsf	Material	Raw ages	Calibrated age	SR	Calibrated age from	Δ Age yr
		^{14}C yr BP	for this study cal yr BP		Crosta et al. (2007) cal yr BP	
2	Humic	2350	1002	0.52	916	86
498	Humic	3235	1951	0.39	1871	80
998	Humic	5175	4388		4314	74
1440	Meteorite	4000	4000		–	–
1498	Humic	6135	5598		5496	102
1998	Humic	6310	5782	0.39	5703	79
2498	Humic	7450	7069	0.39	6984	85
2998	Humic	8775	8344	0.50	8369	–25
3498	Humic	9570	9348	0.32	9208	140
3661	Carbonate	9730	9491		9384	107
3998	Humic	10855	10923		10742	181

Raw dates were calibrated using CALIB 5.0 after removing a reservoir age of 1300 years (Ingólfsson et al., 1998). The rows in boldface show the dates that were discarded (see text). The sedimentation rates used for $^{230}\text{Th}_{\text{xs}}$ calculation are based on the calibrated dates used in the model. Δ ages between Crosta et al. (2007) that used Bard's polynome (Bard et al., 1998) and this study that used CALIB 5.0 (Stuiver et al., 2005) are reported. The maximum age difference between the two age models is less than 200 years.

(Bacon and Anderson, 1982). The ^{230}Th measured in the sediment is corrected for lithogenic and authigenic contributions (See Veeh et al., 2000, for details) and for radioactive in-growth, in order to calculate the amount of ^{230}Th originated from scavenging in the water column, referred to as being “in excess” ($^{230}\text{Th}_{\text{xs}}$). These corrections are based on the estimation of detrital uranium ($^{238}\text{U}_{\text{det}}$), which permits constraint of lithogenic and authigenic contributions. To estimate the $^{238}\text{U}_{\text{det}}$, we used the ^{232}Th concentrations, which have uniquely a detrital origin (Brewer et al., 1980), by multiplying them with the ratio $(^{238}\text{U}/^{232}\text{Th})_{\text{det}} = 0.58$, estimated for the Indian Southern Ocean (Dézileau et al., 2000). This ratio is within the range of ratios measured for other sectors of the Southern Ocean (Francois et al., 1993; Frank, 1996). Authigenic uranium was calculated as the difference between total and detrital uranium, correcting for in-situ growth of ^{230}Th .

Focusing factor (ψ) values are calculated by comparing down-core excess ^{230}Th ($[^{230}\text{Th}_{\text{xs}}]_0$) to the expected flux of ^{230}Th from the overlying water column (Francois et al., 2004):

$$\psi = \frac{\int_{z_1}^{z_2} [^{230}\text{Th}_{\text{xs}}]_0 \rho dz}{\beta h [t_2 - t_1]}$$

where $[^{230}\text{Th}_{\text{xs}}]_0$ is the age-corrected excess ^{230}Th in the sediment in dpm g^{-1} , ρ is the Dry Bulk Density (DBD) in g cm^{-3} , dz is the interval depth in cm, β is the rate of ^{230}Th production from ^{234}U ($\beta = 2.63 \times 10^{-5} \text{ dpm cm}^{-3} \text{ ka}^{-1}$), h is the water depth, and t is the age in ka. ψ greater than 1 indicates focusing. This approach on active hydrodynamic shallow shelves close to sea ice system is not as straightforward as for open marine sites (Francois et al., 2004). Nevertheless, as shown later on, the comparison of $[^{230}\text{Th}_{\text{xs}}]_0$ with other indicators obtained from core MD03-2601, supports the use of ψ as a qualitative proxy of changes in lateral sedimentary input to the core site during the Holocene.

3.2.2. Sortable silt

The mean grain size of the non-cohesive 10–63 μm fraction, sortable silt (\overline{SS}) has been used as a palaeo-flow intensity proxy (McCave and Hall, 2006). Laboratory analyses with a Malvern grain size auto-analyser, performed on the raw sediment, measured the size of the diatoms rather than the terrigenous particles. The opal fraction reaches 35–70% of the total sediment (Crosta et al., 2005) and entire or broken diatoms frustules strongly impact on the grain size value. Similar analyses on NaOH-treated material, though producing a better measure of the size of the terrigenous particles, still show contamination by broken diatoms and possibly loss of terrigenous particles. Therefore, we attempted to determine \overline{SS} from lithic grain microscopic measurements directly on sediment indurated slides. Lithic grain counts, discernible under polarised light, have already been tested on permanent sediment slides and positively compared to titanium content (Denis et al., 2006). The lithic grain data obtained by this method does not allow access to the complete granulometric fraction because of the 5 μm microscopic threshold, but this problem is also encountered using a Coulter Counter or Malvern grain size auto-analyser (McCave and Hall, 2006). Two further limiting factors are apparent when comparing with the more classical methodologies. Firstly, the number of grains analysed is lower, the error bars associated with the calculation of \overline{SS} due to the low numbers of grain counted are shown in Fig. 3. Secondly, the results arise from surface and not volume measurements that can induce two biases. First of all, flat grains occupy the same surface but a reduced volume in comparison to spherical grain, though the two types of grains have a different relationship with current velocity. Most of the grains preserved in core MD03-2601, and

counted under the microscope, are quartz grains and thus are always rounded. We therefore believe that our measurements are relatively unbiased due to shape orientation. Additionally, given the unit change (factor ~ 100) between surface and volume measurements, surface results underestimate the importance of coarser grains versus finer grains on log-normal distribution. This bias induces a lesser differentiation of \overline{SS} between samples. Thereby, the \overline{SS} Holocene trends based on surface measurement should be even more obvious with volume measurement. Despite these limitations, we believe that the mean sortable silt values we produced are valid to identify variations in the bottom current flow over the core site throughout the Holocene. Finally, in the DDUT region, \overline{SS} can be also be influenced by ice rafted transport (Hass, 2002). To consider this point, we have looked the distribution type in the total grain population and have calculated the sorting (σ) and the skewness (Sk) degrees that inform on the dispersion and the symmetry of the total grain population, respectively, and thus identify if there were significant contribution of IRD supply throughout the Holocene.

3.3. Laboratory procedures

The distribution of laminations along the entire core is based on X-ray imagery (Denis et al. (2006).

Aluminium (Al) contents were measured every 32 cm (~ 80 years resolution) by XRF analysis. Full XRF methodology is described in Fitton et al. (1998).

The activity of U series radioelement was determined at 60 depth horizons (Appendix A). Samples of 1–2 g dried sediment were spiked with yield monitors (^{232}U , ^{228}Th) before digestion in mixtures of HCl, HNO_3 , HClO_4 and HF. DBD was measured by determining the dry weight of a known volume of wet sediment with a mean precision of 0.05 g cm^{-3} (Appendix A). The radioelements of interest were purified by ion exchange on anionic resins (Anderson and Fleer, 1982; Sicre et al., 2005). ^{238}U , ^{234}U , ^{232}Th and ^{230}Th activities were determined by α counting (mean 1 σ error: 4.9%, $n = 218$) as previously explained in Schmidt (2006).

Results of grain-size analysis have been obtained by digital analysis of lithic grains, from 101 permanent sediment slides with a mean 40 cm sampling step, corresponding to ~ 100 years resolution (Appendix B). Poly-propylene cubes (8 cm^3) were sampled from core section without disturbing the in situ repartition of the sediment. These sediment samples were thereafter hardened following the method described in Zaragosi et al. (2006). Image acquisition was performed manually using an imagery system composed of a Leica DM600B digital microscope and Leica Qwin 3.0 software on lithic grains larger than 5 μm . Analyses were based on 13.3 mm^2 area (e.g. 25 images). The final results were statistically treated to obtain the most relevant sedimentological parameters such as mean grain-size of the 10–63 μm fraction (\overline{SS}), sorting (σ), and skewness (Sk) with the geometric graphical method, modified after Folk and Ward (1957) (Blott and Pye, 2001). The surface grain areas in each sample are distributed, according to incremental logarithmic step, in 52 and 28 size classes, for the total particles population (e.g. $>5 \mu\text{m}$) and for the 10–63 μm fraction, respectively (given that the average number of counted grains in each sample is 770 and 540 for total and 10–63 μm fraction, respectively, Appendix B). The \overline{SS} confidence intervals are between 0.5 and 2.3 μm , calculated according to Diógenes et al. (2005), which corresponds to a relative accuracy from 2% to 9% on \overline{SS} (Fig. 3E).

Age model, laminae counts, aluminium content, radionuclides and grain size data are available electronically from the Pangaea Data Centre, Bremerhaven, Germany at <http://doi.pangaea.de/10.1594/Pangaea.713060>, -62, -63, -66 and -71, respectively.

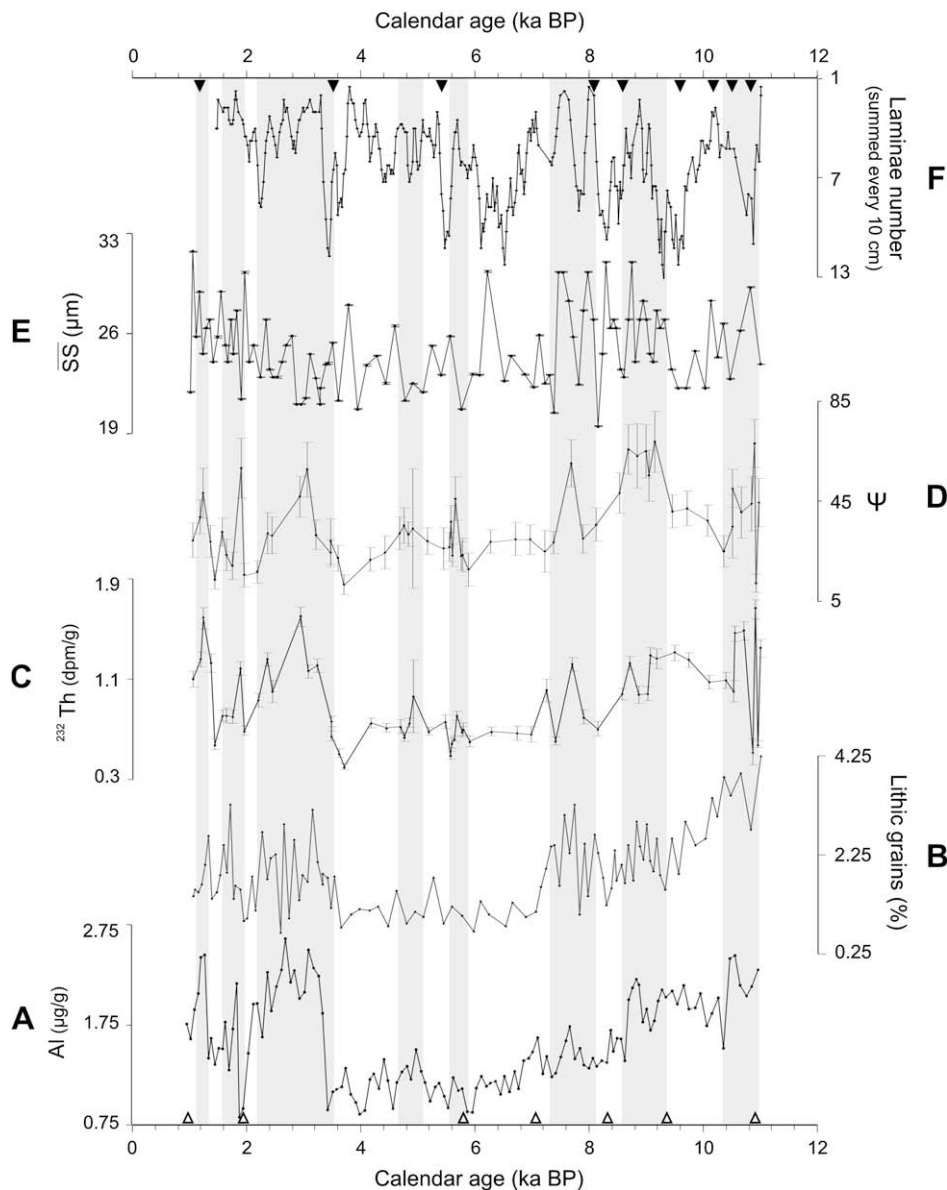


Fig. 3. MD03-2601 data versus time: (A) aluminium content, (B) percentage of the sediment surface held by lithic grains, (C) ^{232}Th , (D) focusing factor (ψ) with error bars ($p < 0.05$), (E) sortable silt (\overline{SS}) with error bars ($p < 0.05$) that are within the symbol points, and (F) 4-point running average of the laminae number summed every 10 cm (note the reversed axis). Shaded areas highlight phases with high focusing and lithic inputs. The white triangles show the position of the ^{14}C dates used to construct the age model (Table 1 and Fig. 2) and the black triangles show the position of the samples chosen for illustrating Fig. 4.

4. Results

Detrital proxies (Al, lithic grain and ^{232}Th contents) show the same Holocene pattern with a general decreasing trend between 11 and 3.5 cal ka BP, interrupted by several rebounds at ~ 11 –10.3, 9.4–8.6 and 8.1–7.3 cal ka BP, and subsequently followed by a three-phase rebound at 3.5–2.2 and 2–1.6 and 1.3–1.1 cal ka BP (Fig. 3A–C). Al and ^{232}Th contents show also a peak at around 5.1–4.8 cal ka BP (Fig. 3A–C).

The focusing factor (ψ) presents relatively high values from 10 to 70 over the last 11 cal ka BP (Fig. 3D). ψ shows similar variations to the detrital proxy records. The highest values of ψ ($\psi \geq 30$) are congruent to the abovementioned peaks in the detrital proxies with a supplementary peaks at 5.9–5.6 cal ka BP (Fig. 3D).

\overline{SS} results show statistically significant variations between 19 μm and 33 μm (Fig. 3E). \overline{SS} general trends display high values

between 11 and 7.4 cal ka BP, followed by a low-stand plateau between 7.4 and 5 cal ka BP and then a continuous increase from 5 to 1 cal ka BP (Fig. 3E). More precisely, the first interval 11–7.4 cal ka BP shows two episodes with higher values of \overline{SS} at ~ 10.8 –10.1 and 9.3–7.4 cal ka BP. The sorting (σ) and the skewness (Sk) show low variations throughout the Holocene around 0.6 and 0, respectively, both on the total fraction ($>5 \mu\text{m}$) and on the 10–63 μm fraction, which indicates very well sorted and symmetrical grain population distributions (Blott and Pye, 2001) (Appendix B). The total grain size population ($>5 \mu\text{m}$) in our laboratory study shows a log-normal distribution (Fig. 4). The more subtle oscillations superimposed on the log-normal distribution plots are reflections of the limited number of grains considered in this study (Fig. 4, Appendix B). Holocene variations, recorded by \overline{SS} , coincide with significant shifts in the principal grain size mode of about 25, 21 and 35 μm (Fig. 4).

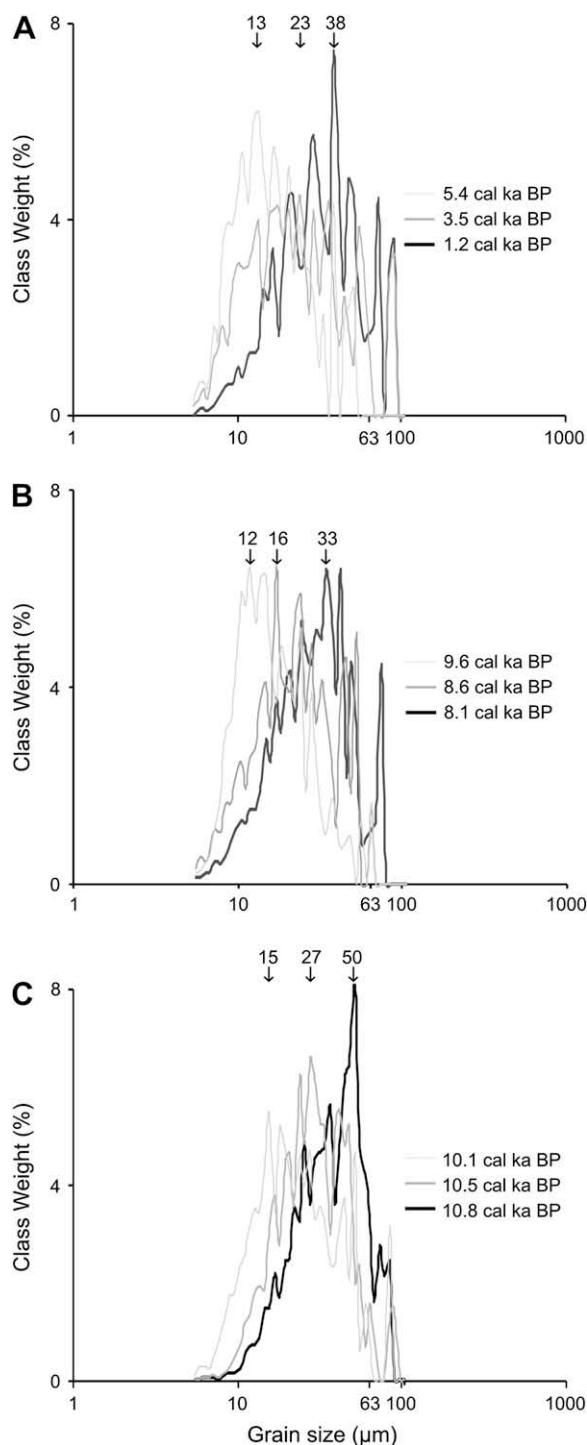


Fig. 4. Logarithmic frequency plots of surface area of the total grain fraction ($>5 \mu\text{m}$) for a selection of samples distributed throughout the core (black triangles in Fig. 3). Surface areas of each sample are distributed in 52 size classes between 5 and $190 \mu\text{m}$, with a logarithmic incremental step. The age of each sample is noted on the right side and the principal mode of grain size is noted at the top of each case. Cases reported in plots A and B describe a decreasing trend of principal mode values whereas the case reported in plot C illustrates an increasing trend of principal mode value.

The number of laminae shows an opposite pattern to sortable silt with low laminae number congruent to larger and more abundant silt fraction (Fig. 3E,F). Low laminae numbers are recorded at around 11, 10.5–9.7, 9.1–8.3, 8.1–6.7 cal ka BP, and a decreasing trend is observed from 6.5–6 cal ka BP to 1 cal ka BP (Fig. 3F).

5. Discussion

5.1. Sedimentary processes

In order to decipher the sedimentary processes associated with changes in detrital content, focusing, and grain size (Figs. 3 and 5B,C), we compare our results with diatom assemblages that document the regional surface ocean conditions (Crosta et al., 2008). Here we use the *F. curta* / *F. kerguelensis* ratio (Fc/Fk ratio), which indicates the predominance of sea ice over ice-free conditions during the growing season (Leventer, 1991, 1998; Armand et al., 2005), reconstructing changes in the spring–summer sea ice cover. *Chaetoceros* resting spore (CRS) relative abundance is used as a proxy of increased surface water stratification (Leventer, 1991; Leventer et al., 1993), tracing the levels of glacier meltwater input (Leventer et al., 2002; Bianchi and Gersonde, 2004; Leventer et al., 2006) (Fig. 5C,D).

5.1.1. Lateral sediment supply

High lateral sedimentary input has affected the core site during the Holocene (Figs. 3D and 5A). Focusing by bottom currents is common on Antarctic continental shelves where bathymetric depressions act as sediment funnels (Camerlenghi et al., 2001; McMullen et al., 2006). The sea-floor bathymetry of the DDUT thus constitutes an area of favourable sediment accumulation. However, the presence of well-preserved seasonal diatom succession in laminations (Denis et al., 2006) demonstrates a local source of sediment focusing during periods of moderate lateral inputs. Superimposed to the baseline values, ψ shows long-term variations, marked by a decreasing trend between 11 and 3.5 cal ka BP and a three-phase rebound after 3.5 cal ka BP (Fig. 3A–C). Within this general pattern, eight periods with higher lateral sedimentary inputs are observed during the Holocene period at ~ 11 – 10.3 , 9.4 – 8.6 , 8.1 – 7.3 , 5.9 – 5.6 , 5.1 – 4.8 , 3.5 – 2.2 , 2 – 1.6 and 1.3 – 1.1 cal ka BP (Fig. 3D), referred to hereafter as events E1 to E8 (Fig. 5A). At both Milankovitch and sub-Milankovitch time scales, except during E4, the lateral input pattern is congruent to terrigenous content changes, as shown by the agreement of the ψ record with the records of detrital proxies (Fig. 3A–D). On the Adélie Land continental shelf, southward and northward bottom transports can act simultaneously to supply terrigenous material to the inner deeper basin (Presti et al., 2003). E1 to E8 events correspond to an increase of cryophilic diatoms in comparison to open-ocean diatoms as evidenced by high Fc/Fk ratio values (Fig. 5A–C), which is not consistent with a supply from the outer shelf. Therefore, we suggest that the most predominant sediment supply at MD03-2601 during E1 to E8 and during the Holocene is from the coast via bottom water transport.

5.1.2. Bottom current

The well-sorted and symmetrical modal distribution of grain size and the small amount of grains superior to $63 \mu\text{m}$ demonstrate that the terrigenous particle transport and deposition is dependent on current-sorting rather than ice-rafted supply (Figs. 3E and 4). Variations of \overline{SS} and principal mode values are thus attributed to significant changes of the bottom current competence during the Holocene. This is further confirmed by the negative correlation between the trends of sortable silt and laminae number records (Fig. 3E,F). The presence of biogenic laminae in marine cores is directly related to export productivity (Leventer et al., 2002) and to the level of bottom water oxygen (Anderson et al., 1990). The distribution of well-preserved laminae in MD03-2601 shows no similarities with productivity variations estimated from ^{230}Th normalised biogenic fluxes (Carson et al., submitted). Therefore, we suggest that the laminae distribution in MD03-2601 is the result of

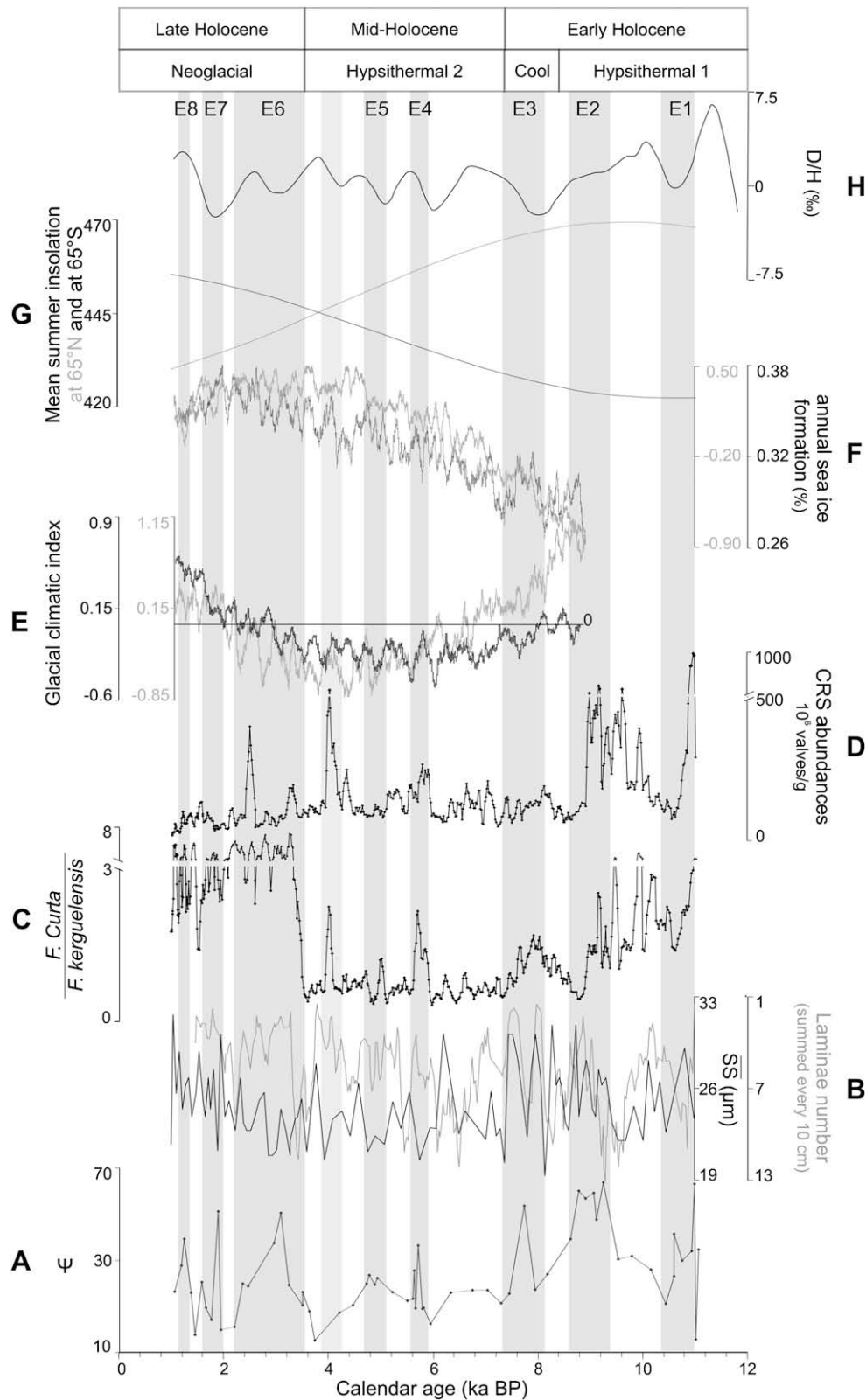


Fig. 5. MD03-2601 data compared to other climatic records versus time: (A) focusing factor (ϕ), (B) deep current proxies: \overline{SS} (black line) and laminae number (4-point running average, grey line), (C) *F. curta* / *F. kerguelensis* ratio, (D) *Chaetoceros* resting spores (CRS) abundances, (E) glacier climatic index from modelled winter precipitation and summer temperature for our area (black line) and for the whole Antarctica (grey line, Renssen et al., 2005a), (F) annual sea ice formation in % to the surface area from modelled summer and winter sea ice cover for the study area (black line) and for the whole southern Ocean (grey line, Renssen et al., 2005a), (G) summer insolation at 65°N and 65°S (Berger and Loutre, 1991), and (H) empirical orthogonal function (EOF) analysis performed on D/H isotopic ratio from 11 East Antarctica ice core sites (Masson et al., 2000). At the top, climatic periods defined by Crosta et al. (2007) are reported. Dark shaded areas, reported from Fig. 3, highlight major changes in the glacier–sea ice–ocean system, called E1 to E8, while the light shaded area at 4 cal ka BP shows a sea ice expansion.

changes in bottom water production, as observed in the Mertz region (Harris et al., 2001). In the Adélie Land region, changes in bottom current intensity is the result of variations in ALBW formation, initiated by HSSW formation during winter sea ice formation. We hereafter focus on the long-term pattern of the \overline{SS} and laminae number records to infer ALBW Holocene dynamics (Fig. 5B). We believe the use of these proxies to interpret ALBW variations at shorter time scales is limited due to (1) calibration control on the proxies and (2) different resolution of the records.

5.1.3. Source and mode of sediment supply

During the Holocene, in particular at E1 to E8 events, variations of lateral terrigenous supply may result from sediment redistribution by bottom currents or from increased sediment load in coastal waters. There were no reworked diatoms and the overall diatom preservation is excellent (i.e. few dissolution) throughout the core (Crosta et al., 2005, 2007, 2008), which argues against sediment remobilisation or bedload transport. Additionally, variations in the focusing factor do not correspond with the changes of ALBW strength throughout the Holocene (Figs. 3 and 5). We therefore believe that both long-term variations of lateral input, in particular events E1 to E8, are the result of increased sediment load in coastal waters.

Glaciers in the Adélie Land region (e.g. Français, Astrolabe and Zélée) have clean upper and basal layers because of the weak aeolian flux during the Holocene (Delmonte et al., 2002; Edwards et al., 2006) and the solid bedrock (Monbeig-Andrieu and Cailleux, 1962; Chamley, 1965; R.-P. Ménot, personal communication, 2008). Therefore, the release of particles by surface or basal melting is low when glacier activity is steady and important during glacier advance-retreat cycles (Gilbert et al., 2002; Oerlemans and Nick, 2006).

We therefore suggest the variations of detrital lateral inputs are related to glacier recession or expansion that release terrigenous particles into the surrounding waters during increased HSSW-ALBW terrigenous charge.

5.2. Palaeoclimatic interpretations

The goal of this study is to document the Holocene movements of Adélie Land glaciers and deep water formation and their links with the sea ice production at Milankovitch and sub-Milankovitch scale. We thus compare our results with records of surface ocean conditions (Crosta et al., 2008), model outputs of Holocene climate evolution for our study area, and High Southern Latitudes (Renssen et al., 2005a), mean summer insolation at 65°N and 65°S (Berger and Loutre, 1991), Antarctic continental climate (Masson et al., 2000), and other investigations of glacier fluctuations in East Antarctica (Ingólfsson et al., 1998; Roberts et al., 2004; Verkulich et al., 2002; Leventer et al., 2006; Fig. 6).

Winter precipitation, atmospheric summer temperature, winter and summer sea ice cover are extracted from the ECBilt-CLIO-VECODE coupled atmosphere–sea ice–ocean–vegetation model experiment, forced by annually varying orbital parameters and greenhouse gas (Renssen et al., 2005a), between 64–70°S and 130–150°E for this study and South of 60°S. It is worth noting that the model output for our study region and the rest of Antarctica (Renssen et al., 2005a) can be examined over the Milankovitch time scale (Fig. 5E,F). The two most important parameters controlling ice mass-balance changes are winter precipitation and mean temperature during the ablation season (Andrews, 1975; Porter, 1975; Lie et al., 2003; Bakke et al., 2008). We have constructed a climatic index based on the normalised variations of the total winter precipitation (from April to October) minus the normalised variations of mean summer temperatures (between November and March) (Fig. 5E).

Positive variations of this glacier climatic index indicate potential favourable periods for glacier advance in the study area and in Antarctica. The annual sea ice cover built up represents the difference between modelled winter and summer sea ice cover in the study area and for the whole Southern Ocean (Fig. 5F).

Deuterium/Hydrogen isotopic records from 11 East Antarctic ice cores have been analysed using an empirical orthogonal function and these results are used as an indicator of climatic trends on the East Antarctic plateau (Masson et al., 2000). Negative values signify colder conditions and positive values signify warmer conditions (Masson et al., 2000) (Fig. 5H).

5.2.1. Milankovitch variability

5.2.1.1. Early Holocene. The decreasing pattern of glacier discharge between 11 and 8.5 cal ka BP likely reflects the terminal glacier recession at the inner part of the Adélie Land continental shelf (Fig. 5A). Larger terrigenous inputs are expected at the onset of glacier recession. Terrigenous supply subsequently decreases during glacier grounding-line retreat and stabilisation. In addition, the decrease of the glacier climatic index confirms a suitable period of glacier retreat occurred between 9 (e.g. start of model experiment) and 7 cal ka BP over Adélie Land margin and around whole Antarctica (Fig. 5E). The additional effect of lower winter precipitations and warmer summer temperature is directly induced by the precessional component of the insolation at low and high southern latitudes (Renssen et al., 2005a; Fig. 5G). The Adélie Land glacier retreat coincides with the timing of the East Antarctic Ice Sheet (EAIS) deglaciation, documented from 13 to 8 cal ka BP (Fig. 6; Goodwin, 1993; Morgan et al., 1997; Ingólfsson et al., 1998; Taylor and McMinn, 2002; Leventer et al., 2006), which was forced by temperature warming and sea level rise (Masson et al., 2000; Masson-Delmotte et al., 2004; Leventer et al., 2006).

The decrease of the Fc/Fk ratio and CRS abundances between 11 and 9 cal ka BP (Fig. 5C,D) suggests the seasonal sea ice cover over the continental shelf was progressively ice free during the spring and summer seasons. Southward migration of the sea ice front associated with glacier grounding-line retreat also occurred between 11 and 9 cal ka BP in the Southern Ocean Atlantic Sector (Bianchi and Gersonde, 2004). During the Early Holocene, the sea ice cycle (e.g. initiation, extent, and duration) was influenced by the combination of global warm conditions (Masson et al., 2000; Masson-Delmotte et al., 2004) and EAIS decay.

High \overline{SS} values and low laminae numbers between 11 and 7.4 cal ka BP argue for an active ALBW (Fig. 5B). The onset of a seasonal sea ice formation on the continental shelf was certainly responsible for the intense ALBW activity. Indeed, the southward migration of the sea ice front associated with glacier grounding-line retreat likely induced a relocation of deep water formation sites on the continental shelf. In the same way, the total retreat of sea ice in the spring–summer season enhanced winter sea ice production on the continental shelf, which increased HSSW, and thus ALBW, formation via sea ice brine rejection (Schmittner, 2003). Our results that suggest a vigorous seasonal sea ice cycle differ from model output during the 9–7 cal ka BP period (Fig. 5B,C,F). The receding glacial conditions affecting the Antarctic climate until 7 cal ka BP are, however, not evidenced by the model that did not “account for the effect of the long-term memory for events that occurred before 9 ka” (Renssen et al., 2005a).

5.2.1.2. Mid to Late Holocene. Between 7 and 3.5 cal ka BP, reduced glacier discharge reflects a stabilisation of the Adélie Land glacier that is in agreement with the flat trend of the glacier climatic index that shows slightly negative values (Fig. 5A–E). Increased snow accumulation rates have been reported since 7 cal ka BP on coastal East Antarctica at Taylor Dome and Law Dome (Steig et al., 2000;

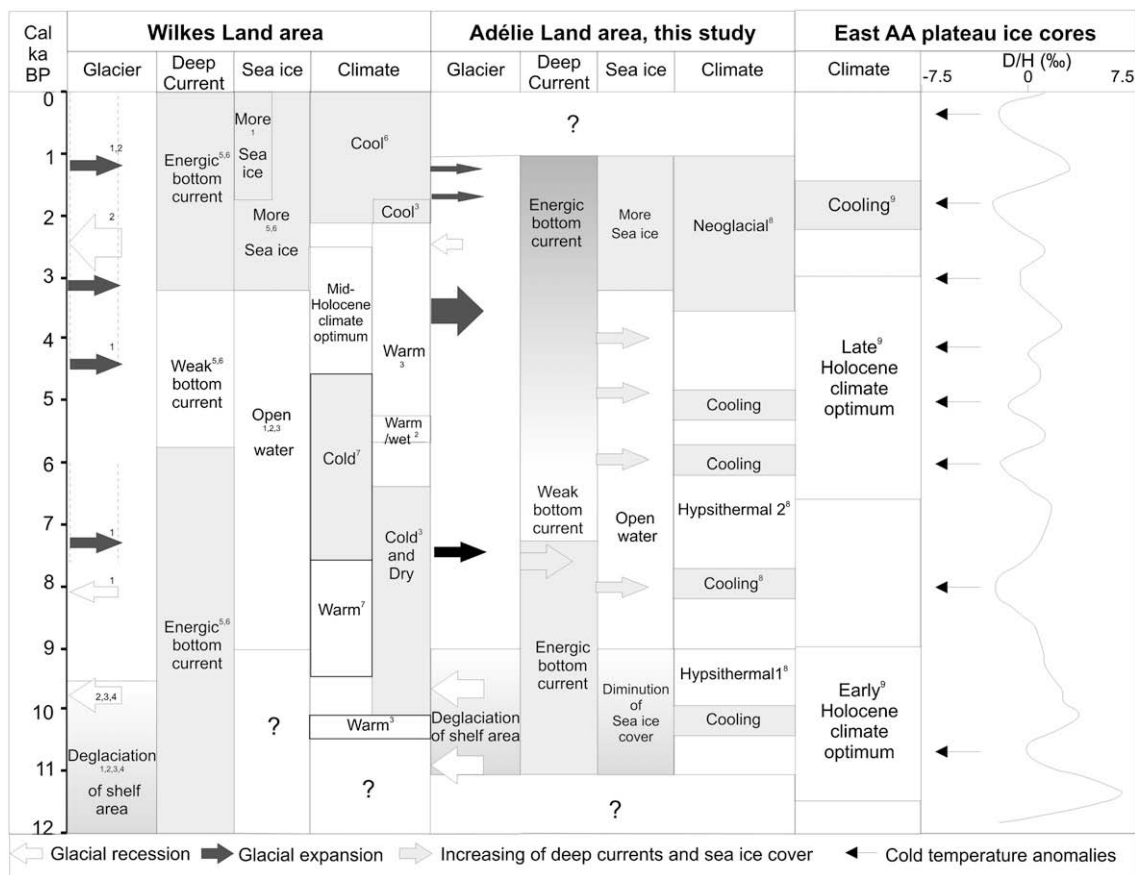


Fig. 6. Synthesis of the different glacier movements, deep current activity, sea ice conditions and climatic trends documented in the Adélie Land area by previous studies (¹Ingólfsson et al., 1998; ²Roberts et al., 2004; ³Verkulich et al., 2002; ⁴Leventer et al., 2006; ⁵Harris et al., 2001; ⁶Presti et al., 2003; ⁷Kulbe et al., 2001; ⁸Crosta et al., 2007) and by this study, in comparison to East Antarctica climate (⁹Masson et al., 2000). The ¹⁴C ka BP dates reported in the publications were converted to calendar ages using Calib 5.0 for comparison with our age model.

van Ommen et al., 2004). These elevated snow accumulation rates have been attributed to enhanced latitudinal insolation gradients since 10 cal ka BP, favouring poleward atmospheric transport (Vimeux et al., 2001) and thus enhanced precipitations over Antarctica (Rind, 2000). Increased snow fall was likely compensated by greater ice melting due to warmer summer atmospheric temperatures (Renssen et al., 2005a), thus maintaining a stable glacier mass balance.

The Fc/Fk ratio and CRS abundances show low steady values (Fig. 5C,D), which infers an earlier sea ice waning and a longer ice-free season (Crosta et al., 2008). The reduced amount of easy-to-freeze runoffs, in comparison to deglacial conditions, may explain the lower Fc/Fk ratio values and CRS abundances and the reduced seasonal sea ice cycle though the Mid Holocene presents cooler conditions than during the Early Holocene (Masson et al., 2000; Masson-Delmotte et al., 2004).

Since 3.5 cal ka BP, glacier discharges has increased concomitantly with the glacier climatic index (Fig. 5A–E). The decrease in spring–summer surface temperature since 4–3.5 cal ka BP (Renssen et al., 2005a) has reduced the melting of winter snow and may have permitted the expansion of the glacier grounding-line during the Late Holocene. Studies on Law Dome and in the coastal margin of Adélie Land, show similar readvance of glaciers since 4 cal ka BP, forced by accumulation rate changes (Goodwin, 1998). The rapid increase of the spring–summer sea ice cover is also in line with this orbital forcing favourable to a latter sea ice waning and a shorter ice-free season (Fig. 5C; Renssen et al., 2005a; Crosta et al., 2008).

Both laminae number and sortable silt records indicate a progressive increase of the ALBW activity between 6.5–5 and 1 cal ka BP (Fig. 5B). The ALBW pattern is remarkably similar to modelled yearly sea ice formation since 7 cal ka BP (Fig. 5F), demonstrating the importance of the seasonal sea ice cycle on the deep water formation.

5.2.1.3. Larger implications. The long-term evolution of Adélie Land glaciers during the Holocene appears forced by precessional orbital changes, evident from the sea ice sub-system (Crosta et al., 2008). The strong synchronicity of these two climatic components argues for a similar sensitivity to the forcing factors such as seasonality and spring–summer temperature. This indicates a strong interconnection via positive feedbacks such as the albedo, which can affect the amplitude of their responses to climate changes. Adélie Land glaciers show a coherent pattern with model prediction for the whole of Antarctica (Fig. 5E), with most glaciers around Antarctica (Fig. 6; Ingólfsson et al., 1998; Leventer et al., 2006; Yoon et al., 2007) and around the world (Solomina et al., 2008 and references therein). Perhaps, some strong specificity of local climate and bedrock topography can induce time lag (Goodwin, 1998).

In-situ measurements indicated that the ALBW can supply 25% of the Antarctic Bottom Water (AABW) (Gordon and Tchernia, 1972; Rintoul, 1998), in agreement with model output (Baines and Condie, 1998; Goosse et al., 2001). If the close relationship between deep water formation and sea ice formation observed off Adélie Land is valid for the whole Antarctic Ocean (Fig. 5F; Renssen et al.,

2005a), our results suggest a long-term increase of AABW formation between 6.5–5 and 1 cal ka BP. Although no other high-resolution Antarctic marine records of deep water formation exist, studies of sediment facies (Harris et al., 2001; Presti et al., 2003) and of grain size sorting (Yoon et al., 2007) similarly suggest enhanced bottom water formation during Early and Late Holocene in the Mertz area (Fig. 6) and the northern Antarctic Peninsula, respectively. Accordingly, $\delta^{13}\text{C}$ records measured on benthic foraminifera in several cores from the East Atlantic showed enhanced AABW flow since 7.5 cal ka BP, which was concomitant to a Mid-Holocene reduction of the North Atlantic Deep Water (NADW) ventilation (Sarnthein et al., 1994). Indeed, in the Northern Hemisphere, NADW contribution shows intensification between 10 and 6.5 cal ka BP, followed by a decreasing trend (Oppo et al., 2003). A slowing down of the northern end-member of the thermohaline circulation is also suggested since 7 cal ka BP, based on proxies related to surface and bottom waters (Duplessy et al., 2001; Rasmussen et al., 2002; Hall et al., 2004; Solignac et al., 2004), and during the Mid Holocene, based on model experiment (Ganopolski et al., 1998). To summarise, these results may suggest that: (1) a similar behaviour of deep water formation in both hemispheres occurs during the Early Holocene as a result of the onset of post-glacial seasonal sea ice cycle and, thus, re-initiation of deep water formation, and (2) an opposite behaviour of deep water formation since the Mid Holocene as a result of opposite precessional insolation trends that lead to increase seasonality in the Southern Hemisphere (Renssen et al., 2005a), and to decrease seasonality in the Northern Hemisphere (Renssen et al., 2005b; Naughton et al., 2007) (Fig. 5H).

5.2.2. Sub-Milankovitch variability

At the sub-orbital time scale, the glaciers, and sea ice climatic sub-systems demonstrate millennial oscillations that are well expressed during E1 to E8. These occurred within different climatic regimes: the warm Hypsithermal, the cool period and the colder Neoglacial (Fig. 5; Crosta et al., 2007). Interpretations are within the uncertainties of the age model.

5.2.2.1. Hypsithermal 1 (11–8.5 cal ka BP). During the deglaciation, we observe two events of high terrigenous input E1 and E2 dated at 11–10.3 cal ka BP and 9.4–8.6 cal ka BP (Fig. 5A). High CRS abundances occur at the beginning of E1 and before E2 until 9 cal ka BP (Fig. 5D). The focusing and CRS records would suggest there was increased surface water stratification during enhanced glacier meltwater input. High values of the Fc/Fk ratio also occurred until 9 cal ka BP, indicating persistent spring–summer sea ice cover during the warmer climate of the Early Holocene (Masson et al., 2000; Masson-Delmotte et al., 2004) (Fig. 5C). We suggest that glacier meltwaters decreased the surface salinity, which promoted sea ice freezing that persisted during diatom growing seasons. As negative feedback, sea ice formation isolated the atmosphere from the warmer ocean surface and increased the albedo, thus resulting in an additional cooling.

The CRS record also indicates that ice-melting pre-dated the effective glacier grounding-line recession off Adélie Land evidenced by E1 and E2 (Fig. 5A). Initiation of the ice melting (Fig. 5D) is in phase with warming phases recorded in East Antarctica (Fig. 5H) while E1 and E2 occurred 500 and 1000 years later respectively, during cooling phases (Masson et al., 2000) in relation to the great inertia of glacier mass-balances. The reaction time of ice sheet mass balance was calculated to be around 500 years at the ice cap margin (Goodwin, 1996, 1998). Massive freshwater discharges may have initiated or contributed to the two cooling events recorded over East Antarctica during the Early Holocene (Masson et al., 2000), in agreement with modelled climatic impacts of Antarctic

freshwater runoffs (Mikolajewicz, 1998; Richardson et al., 2005; Stouffer et al., 2007).

5.2.2.2. Cool event (8.5–7 cal ka BP). During E3 (8.1–7.3 cal ka BP), the peak in focusing and terrigenous content is associated with low values of CRS abundances (Fig. 5A–D). These results suggest that the high terrigenous input is not related to glacier recession. Conversely, E3 is synchronous to increased sea ice cover as shown by higher values of the Fc/Fk ratio between 8.6 and 7.3 cal ka BP (Fig. 5C–H). E3 is also concomitant to one of the strongest Holocene atmospheric cooling over the East Antarctica plateau (Masson et al., 2000; Fig. 5H). This cooling may have triggered a glacier advance and sea ice expansion during the deglaciation. Glacier and sea ice advance during E3 are in phase with sea ice expansion recorded between 8 and 7 cal ka BP in the Atlantic sector of the Southern Ocean (van Beek et al., 2002; Bianchi and Gersonde, 2004; Nielsen et al., 2004), and follow the multi-centennial cold event at 8.2 cal ka BP observed around the globe (Mayewski et al., 2004; Rohling and Pälike, 2005). The end of E3 is marked by a relatively abrupt decrease in terrigenous content, focusing factor and sortable silt values, which is probably related to the return of warmer conditions at the onset of the Hypsithermal 2. This shift post-dates the abrupt Early to Mid-Holocene climatic transition (EMHT), recorded between 8.3 and 7.8 cal ka BP (Stager and Mayewski, 1997; Stager et al., 2003). This cool event and the following EMTH recorded here at high southern latitudes follow the climatic changes at low and high northern latitudes, supporting the idea of a coherent Holocene global pattern (Mayewski et al., 2004).

5.2.2.3. Hypsithermal 2 (7–3.5 cal ka BP). During the Hypsithermal 2, the ‘steady’ state of Adélie Land glaciers is interrupted by E4 and E5 at 5.9–5.6 cal ka BP and 5.1–4.8 cal ka BP (Fig. 5A). E4 is associated with higher values of the Fc/Fk ratio (Fig. 5C) and to a short peak in CRS abundances (Fig. 5D). Conversely, the terrigenous proxies show no increase during E4 (Fig. 3). On the other hand, E5 is associated to low values of the Fc/Fk ratio and CRS abundances but to greater values of Al content and ^{232}Th (Figs. 3 and 5). Both events are lagging small atmospheric cooling periods by 200–100 years (Figs. 2 and 5H; Masson et al., 2000). It is therefore believed that the cooling events triggered short-lived glacier re-advances and sea-ice waxing, which resulted in the small influx of terrigenous particles.

A third cooling event is evidenced in the diatom records at around 4 cal ka BP but is not reflected in the ψ , and the terrigenous proxies (Figs. 3 and 5A–D). This event may be triggered by the small atmospheric cooling centred at 4.2 cal ka BP (Fig. 5H; Masson et al., 2000). Our data indicate that this small cooling impacted the sea ice cover but had little effect on the glacier system of Adélie Land.

5.2.2.4. Neoglacial (3.5–1 cal ka BP). Three events of high focusing, E6 at 3.5–2.2 cal ka BP, E7 at 2–1.6 cal ka BP and E8 at 1.3–1.1 cal ka BP, are found during the Neoglacial period (Fig. 5A). These three events are associated with high terrigenous input (Fig. 3) implying important glacier discharges. These events are also concomitant to the highest Holocene values of the Fc/Fk ratio (Fig. 5C) but to non-significant changes of CRS abundances except for a short-lived peak at 2.4 cal ka BP (Fig. 5D). Given these data, we propose that E6, E7 and E8, events of terrigenous discharge, represent episodes of glacier and sea ice expansion rather than retreat because they are associated with spring–summer sea ice assemblages rather than with glacier meltwater assemblages. E6 was triggered by a small temperature fall as recorded over East Antarctica (Fig. 5H; Masson et al., 2000). It is possible that the amplitude of E6 is due to the increase of the glacier climatic index since 3.8 cal ka BP (Fig. 5E) that amplified the response of the glacier system, and to the concomitant sea ice expansion that

provided a positive feedback. A similar expansion of Wilkes Land glaciers has been reported at ~ 3.3 ^{14}C ka BP (ca 3.5 cal ka BP) for the Mertz and the Ninnis glaciers (Fig. 6; McMullen et al., 2006). After a stabilisation, or even a small retreat of the glacier system between 3 cal ka BP and 2 cal ka BP that coincides with the ice margin retreat identified in Windmill island (101°E) between 2.8 and 1.9 ^{14}C ka BP (ca 2.9 cal ka BP and 1.85 cal ka BP) (Roberts et al., 2004), we observe two small glacier expansions. E7 lasted around 400 years and is triggered by an important temperature fall whereas E8 lasted 200 years and is congruent to a temperature rise (Fig. 5H; Masson et al., 2000). Additional work is necessary to understand the apparent paradox between warm atmospheric conditions, glacier advance and sea ice expansion during E8.

6. Conclusions

Major Holocene changes in lateral terrigenous inputs in the Adélie Land margin were triggered by the retreat and/or advance of the nearby glaciers. High-resolution analyses of grain size, diatom assemblages together with the quantification of well-preserved laminae in MD03-2601 provide complementary information about deep water formation and sea ice cover changes in the Adélie Land region. All records show long-term and millennial variability of the glacier–sea ice–oceanic systems into three distinct features:

- An Early Holocene period (11–8.5 cal ka BP) when glacier and sea ice retreat have favoured increased bottom water formation. At millennial time scale, two events of effective glacier recessions at 10.5 cal ka BP and 8.9 cal ka BP occurred after warming phases. Intense meltwater outflow associated with glacier recessions stratified the surface waters and enhanced the persistence of spring–summer sea ice. Increased sea ice cover provided a negative feedback on East Antarctic atmospheric temperatures by increasing albedo.
- One event of glacier advance at 7.7 cal ka BP occurred during a cooling phase (8.5–7 cal ka BP), documented in East Antarctica (Masson et al., 2000), in the Atlantic Sector of Southern Ocean (Bianchi and Gersonde, 2004) and around the world (Mayewski et al., 2004). Sea ice expansion during the cool event provided a positive feedback on East Antarctic atmospheric temperatures.
- A Mid- to Late Holocene (7–1 cal ka BP), when we observe an orbital-forced transition from a relatively ‘steady’ state of the glacier and sea ice systems to their major expansion after 3.5 cal ka BP. Increasing sea ice seasonality, by complete spring–summer retreat and active winter production, concomitantly enhanced deep water formation in DDUT due to greater brine rejection. At the millennial time scale, five glacier–sea ice advances triggered by atmospheric cooling on East Antarctica plateau occurred during the Mid- to Late Holocene.

The interconnections evident between glacier, sea ice and ocean climatic components point out the important impact of sea ice as a link between glacier and deep water dynamics, and its complex role because of its strong sensitivity to seasonality. Future work should improve the reconstruction of centennial-to-millennial oscillations of glaciers and sea ice in the Adélie Land region during the Holocene and the understanding of these components on the ALBW signal at this time scale.

Acknowledgements

We thank Elodie Marchès and Samuel Toucanne for their help in the understanding of sedimentological processes. We are grateful

to both of the anonymous reviewers for their constructive suggestions. We personally thank people from Images X (CADO) cruise and from NSF-funded NBP0101 cruise for data and suggestions concerning the Dumont d’Urville Trough. Financial support for this study was provided by TARDHOL project through the national PNEDC Program (INSU-CNRS) with the logistic support of the French IPEV (Institut Paul Emile Victor), the International Marine Past Global Change Study (IMAGES) and the ACI JC ARTTE. This is an EPOC contribution No. 1721.

Appendix A. Supplemental material

Supplementary information for this manuscript can be downloaded at doi: [10.1016/j.quascirev.2008.12.024](https://doi.org/10.1016/j.quascirev.2008.12.024).

References

- Adolphs, U., Wendler, A., 1995. A pilot-study on the interactions between katabatic winds and polynyas at the Adélie coast, eastern Antarctica. *Antarctic Sciences* 7, 307–314.
- Anderson, R.F., Fleer, A.P., 1982. Determination of natural actinides and plutonium in marine particulate matter. *Analytical Chemistry* 54, 1142–1147.
- Anderson, R.Y., Linsley, B.K., Gardner, J.V., 1990. Expression of seasonal and ENSO forcing in climatic variability at lower than ENSO frequencies: evidence from Pleistocene marine varves off California. *Palaeogeography, Palaeoclimatology, Palaeoecology* 78, 287–300.
- Andrews, J.T., 1975. *Glacial Systems. An Approach to Glaciers and their Environments*. Duxbury Press, North Scituate.
- Armand, L.K., Crosta, X., Romero, O., Pichon, J.J., 2005. The biogeography of major diatom taxa in Southern Ocean sediments: 1. Sea ice related species. *Palaeogeography, Palaeoclimatology, Palaeoecology* 223, 93–126.
- Arrigo, K.R., van Dijken, G.L., 2003. Phytoplankton dynamics within 37 Antarctic coastal polynya systems. *Journal of Geophysical Research* 108 (C8), 3271. doi:10.1029/2002JC001739, 2003.
- Bacon, M.P., Anderson, R.F., 1982. Distribution of thorium isotopes between dissolved and particulate forms in the deep sea. *Journal of Geophysical Research* 87, 2045–2056.
- Baines, P.G., Condie, S., 1998. Observations and modelling of Antarctic downslope flows: a review. In: Jacobs, S.S., Weiss, R. (Eds.), *Ocean, Ice and Atmosphere: Interactions at the Antarctic Continental Margin*. Antarctic Research Series, vol. 75. American Geophysical Union, pp. 29–49.
- Bakke, J., Lie, O., Dahl, S.O., Nesje, A., Bjune, A.E., 2008. Strength and spatial patterns of the Holocene wintertime westerlies in the NE Atlantic region. *Global and Planetary Change* 60, 28–41.
- Bard, E., Arnold, M., et al., 1998. Radiocarbon calibration by means of mass spectrometric Th-230/U-234 and C-14 ages of corals: an updated database including samples from Barbados, Mururoa and Tahiti. *Radiocarbon* 40 (3), 1085–1092.
- Beckmann, A., Pereira, A.F., 2003. Lateral tidal mixing in the Antarctic marginal seas. *Ocean Dynamics* 53, 21–26.
- Berger, A., Loutre, M.F., 1991. Insolation values for the climate of the last 10 million years. *Quaternary Science Reviews* 10 (4), 297–317.
- Bianchi, C., Gersonde, R., 2004. Climate evolution at the last deglaciation: the role of the Southern Ocean. *Earth and Planetary Science Letters* 228, 407–424.
- Bindoff, N.L., Rintoul, S.R., Massom, R., 2000a. Bottom water formation and polynyas in Adélie Land, Antarctica. *Papers and Proceedings of the Royal Society of Tasmania* 133 (3), 51–57.
- Bindoff, N.L., Rosenberg, M.A., Warner, M.J., 2000b. On the circulation and water masses over the Antarctic continental slope and rise between 80 and 150°E. *Deep-Sea Research II* 47, 2299–2326.
- Blott, S.J., Pye, K., 2001. GRADISTAT: a grain size distribution and statistics package for the analysis of unconsolidated sediments. *Earth Surface Processes and Landforms* 26, 1237–1248.
- Brewer, P.G., Nozaki, Y., Spencer, D., Fleer, A.P., 1980. Sediment trap experiments in the deep North Atlantic: isotopic and elemental fluxes. *Journal of Marine Research* 38, 703–728.
- Camerlenghi, A., Domack, E., Rebesco, M., Gilbert, R., Ishman, S., Leventer, A., Brachfeld, S., Drake, A., 2001. Glacial morphology and post-glacial contours in northern Prince Gustav Channel (NW Weddell Sea, Antarctica). *Marine Geophysical Researches* 22, 417–443.
- Carson, D.S., Denis, D., Ganeshram, R.S., Crosta, X., Schmidt, S., submitted for publication. Reconstructing paleoproductivity throughout the Holocene: A case study from Adélie Land, East Antarctica. *Geochimica et Cosmochimica Acta*
- Cavaliere, D.J., Martin, S., 1985. A passive microwave study of polynyas along the Antarctic Wilkes Land Coast. edited by S.S. Jacobs in *Oceanology of the Antarctic Continental Shelf*, Antarctic Research. Series 43, 177–201.
- Chamley, H., 1965. Observations sur quelques sédiments marins prélevés près des côtes de Terre Adélie. *Rec. Trav. Stat. Mar. Endoumé* 36 (52), 215–228.
- Chen, J.H., Wasserburg, G.J., von Damm, K.L., Edmond, J.M., 1986. The U-Th-Pb systematics in hot springs on the East Pacific Rise at 21°N and Guaymas Basin. *Geochimica Cosmochimica Acta* 50, 2467–2479.

- Courty, M.A., Cortese, G., Crisci, A., Crosta, X., Dewever, P., Fedoroff, M., Guichard, F., Mermoux, M., Michel, E., Smith, D., Thiemens, M., 2007. Impact fingerprints of the 4 kyr BP dust event based on archaeological, soil, lake and marine archives. General Assembly of the European Geosciences Union, Vienna, Austria. 16–20 April 2007.
- Crosta, X., Crespin, J., Billy, I., Ther, O., 2005. Major factors controlling Holocene $\delta^{13}\text{C}_{\text{org}}$ changes in a seasonal sea ice environment, Adélie Land, East Antarctica. *Global Biogeochemical Cycles* 19, GB4029. DOI: 4010.1029/2004GB002426
- Crosta, X., Debret, M., Denis, D., Courty, M.A., Ther, O., 2007. Holocene long- and short-term climate changes off Adélie Land, East Antarctica. *Geochemistry, Geophysics, and Geosystems* 8, Q11009. doi:10.1029/2007GC001718.
- Crosta, X., Denis, D., Ther, O., 2008. Sea ice seasonality during the Holocene, Adélie Land, East Antarctica. *Marine Micropaleontology* 66, 222–232.
- DeConto, R., Pollard, D., Harwood, D., 2007. Sea ice feedback and Cenozoic evolution of Antarctic climate and ice sheets. *Paleoceanography* 22, PA3214. 3210.1029/2006PA001350.
- Delmonte, B., Petit, J.R., Maggi, V., 2002. LGM-Holocene changes and Holocene millennial-scale oscillations of dust particles in the EPICA Dome C ice core, East Antarctica. *Annals of Glaciology* 35, 306–312.
- Denis, D., Crosta, X., Zaragosi, S., Martin, B., Mas, V., 2006. Seasonal and sub-seasonal climate changes recorded in laminated diatom ooze sediments, Adélie Land, East Antarctica. *The Holocene* 16, 1143–1153.
- Dézileau, L., Bareille, G., Reiss, J.L., Lemoine, F., 2000. Evidence for strong sediment redistribution by bottom currents along the southeast Indian Ridge. *Deep-Sea Research* 47, 1899–1936.
- Diógenes, A.N., Hoff, E.A., Fernandes, C.P., 2005. Grain size measurement by image analysis: An application in the ceramic and in the metallic industries. Proceedings of COBEM 2005, 18th International Congress of Mechanical Engineering, November 6–11, 2005, Ouro Preto, MG.
- Duplessy, J.C., Ivanova, E., Murdmaa, I., Paterne, M., Labeyrie, L., 2001. Holocene paleoceanography of the northern Barents Sea and variations of the northward heat transport by the Atlantic Ocean. *Boreas* 30, 1–16.
- Edwards, R., Sedwick, P., Morgan, V., Boutron, C., 2006. Iron in ice cores from Law Dome: A record of atmospheric iron deposition for maritime East Antarctica during the Holocene and Last Glacial Maximum. *Geochemistry, Geophysics, and Geosystems* 7 (12), Q12Q01. doi:10.1029/2006GC001307.
- Escutia, C., Warnke, D., Acton, G.D., Barcena, A., Burckle, L., Canals, M., Frazee, C.S., 2003. Sediment distribution and sedimentary processes across the Antarctic Wilkes Land margin during the Quaternary. *Deep-Sea Research II* 50, 1481–1508.
- Fitton, J.G., Saunders, A.D., Larsen, L.M., Hardarson, B.S., Norry, M.J., 1998. Volcanic rocks from the southeast Greenland margin at 63°N: Composition, petrogenesis, and mantle sources. Proceedings of the Ocean Drilling Program. *Scientific Results* 152, 331–350.
- Folk, R.L., Ward, W.C., 1957. Brazos River bar: a study in the significance of grain size parameters. *Journal of Sedimentary Petrology* 27, 3–26.
- Francois, R., Bacon, M.P., Altabet, M.A., 1993. Glacial/interglacial changes in sediment rain rate in the SW Indian sector of subantarctic waters as recorded by 230Th, 231Pa, U, and 15N. *Paleoceanography* 8, 611–629.
- Francois, R., Frank, M., van de Loeff, M.M.R., Bacon, M.P., 2004. 230Th normalization: An essential tool for interpreting sedimentary fluxes during the late Quaternary. *Paleoceanography* 19, PA1018. doi:10.1029/PA000939.
- Frank, M., 1996. Reconstruction of late Quaternary environmental conditions applying the natural radionuclides 230Th, 10Be, 231Pa and 238U: A study of deep-sea sediments from the eastern Atlantic sector of the Antarctic Circumpolar Current system. Reports on Polar Research 186, 136.
- Ganopolski, A., Kubatzki, C., Claussen, M., Brovkin, V., Petoukhov, V., 1998. The influence of vegetation–atmosphere–ocean interaction on climate during the mid-holocene. *Science* 280, 1916–1919.
- Gilbert, R., Nielsen, N., Moller, H., Desloges, J.R., Rasch, M., 2002. Glacimarine sedimentation in Kangerdluk (Disko Fjord), West Greenland, in response to a surging glacier. *Marine Geology* 191, 1–18.
- Goodwin, I.D., 1993. Holocene deglaciation, sea-level change, and the emergence of the Windmill Islands, Budd Coast, Antarctica. *Quaternary Research* 40, 70–80.
- Goodwin, 1996. A mid to late Holocene readvance of the Law Dome ice margin, Budd Coast, East Antarctica. *Antarctic Science* 8, 395–406.
- Goodwin, 1998. Did changes in Antarctic ice volume influence Late Holocene sea-level lowering? *Quaternary Science Reviews* 17, 319–332.
- Goosse, H., Campin, J.-M., Tartini, B., 2001. The sources of Antarctic bottom water in a global ice-ocean model. *Ocean Modelling* 3, 51–65.
- Gordon, A.L., Tchernia, P., 1972. Waters of the continental margin off Adélie coast, Antarctica. In: Hayes, D.E. (Ed.), *Antarctic Oceanology: II. The Australian–New Zealand Sector*. Antarctic Research Series, vol. 19, pp. 59–70.
- Hall, I.R., McCave, I.N., 2000. Palaeocurrent reconstruction, sediment and thorium focussing on the Iberian margin over the last 140 ka. *Earth and Planetary Science Letters* 178, 151–164.
- Hall, I.R., Bianchi, G.G., Evans, J.R., 2004. Centennial to millennial scale Holocene climate-deep water linkage in the North Atlantic. *Quaternary Science Reviews* 23 (14–15), 1529–1536.
- Harris, P.T., Beaman, R.J., 2003. Processes controlling the formation of the Mertz Drift, George Vth continental shelf, East Antarctica: evidence from 3.5 kHz sub-bottom profiling and sediment cores. *Deep Sea Research Part II: Topical Studies in Oceanography* 50, 1463–1480.
- Harris, P.T., Brancolini, G., Armand, L., Busetti, M., Beaman, R.J., Giorgetti, G., Presti, M., Trincardi, F., 2001. Continental shelf drift deposit indicates non-steady state Antarctic bottom water production in the Holocene. *Marine Geology* 179, 1–8.
- Hass, H.C., 2002. A method to reduce the influence of ice-rafted debris on a grain-size record from the northern Fram Strait, Arctic Ocean. *Polar Research* 21, 299–306.
- Hodell, D.A., Kanfoush, S.L., Shemesh, A., Crosta, X., Charles, C.D., Guilderson, T.P., 2001. Abrupt cooling of Antarctic surface waters and sea ice expansion in the South Atlantic sector of the Southern Ocean at 5000 cal yr B.P. *Quaternary Research* 56, 191–198.
- Hughen, K.A., Baillie, M.G.L., Bard, E., Bayliss, A., Beck, J.W., Bertrand, C.J.H., Blackwell, P.G., Buck, C.E., Burr, G.S., Cutler, K.B., Damon, P.E., Edwards, R.L., Fairbanks, R.G., Friedrich, M., Guilderson, T.P., Kromer, B., McCormac, F.G., Manning, S.W., Bronk Ramsey, C., Reimer, P.J., Reimer, R.W., Remmele, S., Southon, J.R., Stuiver, M., Talamo, S., Taylor, F.W., van der Plicht, J., Weyhenmeyer, C.E., 2004. Marine04 Marine radiocarbon age calibration, 26–0 ka BP. *Radiocarbon* 46, 1059–1086.
- Ingólfsson, O., Hjort, C., 1999. The Antarctic contribution to Holocene global sea level rise. *Polar Research* 18, 323–330.
- Ingólfsson, O., Hjort, C., Berkman, P.A., Björck, S., Colhoun, E., Goodwin, I.D., Hall, B., Hirakawa, K., Melles, M., Möller, P., Prentice, M.L., 1998. Antarctic glacial history since the last glacial maximum: an overview of the record on land. *Antarctic Science* 10, 326–344.
- Joughin, I., Padman, L., 2003. Melting and freezing beneath Filchner-Ronne Ice Shelf, Antarctica. *Geophysical Research Letters* 30, 1477. doi: 1410.1029/2003GL016941.
- Kulbe, T., Melles, M., Verkulich, S.R., Pushina, Z.V., 2001. East Antarctic climate and environmental variability over the last 9400 years inferred from marine sediments of the Bungee Oasis. *Arctic, Antarctic and Alpine Research* 33, 223–230.
- Leventer, A., 1991. Sediment trap diatom assemblages from the northern Antarctic Peninsula region. *Deep Sea Research Part I: Oceanographic Research Papers* 38, 1127–1143.
- Leventer, A., 1992. Modern distribution of diatoms in sediments from the George V Coast, Antarctica. *Marine Micropaleontology* 19, 315–332.
- Leventer, A., 1998. The fate of Antarctic “sea-ice diatoms” and their use as paleoenvironmental indicators. In: Lizotte, M., Arrigo, K. (Eds.), *Antarctic Sea Ice Biological Processes, Interactions and Variability*. American Geophysical Union Antarctic Research Series, vol. 73, pp. 121–137.
- Leventer, A., Dunbar, R.B., DeMaster, D.J., 1993. Diatom evidence for Late Holocene climatic events in Granite Harbor, Antarctica. *Paleoceanography* 8, 373–386.
- Leventer, A., Domack, E., Barkouk, A., McAndrews, B., Murray, J., 2002. Laminations from the Palmer Deep: A diatom-based interpretation. *Paleoceanography* 17 (2) 3-1 to 3-15.
- Leventer, A., Domack, E., Dunbar, R., Pike, J., Stickley, C., Maddison, E., Brachfeld, S., Manley, P., McClennen, C., 2006. Marine sediment record from the East Antarctic margin reveals dynamics of ice sheet recession. *Geological Society of America Today* 16 (12), 4. doi:10.1130/GSAT01612A.1.
- Lie, Ø., Olaf Dahl, S., Nesje, A., 2003. A theoretical approach to glacier equilibrium-line altitudes using meteorological data and glacier mass-balance records from southern Norway. *Holocene* 13, 365–372.
- Masson, R.A., Harris, P.T., Michael, K.J., Potter, M.J., 1998. The distribution and formative processes of latent-heat polynyas in East Antarctica. *Annals of Glaciology* 27, 420–426.
- Masson, V., Vimeux, F., Jouzel, J., Morgan, V., Delmotte, M., Ciais, P., Hammer, C., Johnsen, S., Lipenkov, Y., Mosley-Thompson, V.E., Petit, J.-R., Steig, E.J., Stievenard, M.R.V., 2000. Holocene climatic variability in Antarctica: what can be inferred from 11 ice core isotopic records? *Quaternary Research* 54, 348–358.
- Masson-Delmotte, V., Stenni, B., Jouzel, J., 2004. Common millennial-scale variability of Antarctic and Southern Ocean temperatures during the past 5000 years reconstructed from the EPICA Dome C ice core. *The Holocene* 14 (2), 145–151.
- Mayewski, P.A., Rohling, E.J., Curt Stager, J., Karlen, W., Maasch, K.A., David Meeker, L., Meyerson, E.A., Gasse, F., van Kreveld, S., Holmgren, K., Lee-Thorp, J., Rosqvist, G., Rack, F., Staubwasser, M., Schneider, R.R., Steig, E.J., 2004. Holocene climate variability. *Quaternary Research* 62, 243–255.
- McCave, I.N., Hall, I.R., 2006. Size sorting in marine muds: Processes, pitfalls, and prospects for paleoflow-speed proxies. *Geochemistry, Geophysics, Geosystems* 7, Q10N05. doi:10.1029/2006GC001284.
- McMullen, K., Domack, E., Leventer, A., Olson, C., Dunbar, R., Brachfeld, S., 2006. Glacial morphology and sediment formation in the Mertz Trough, East Antarctica. *Palaeogeography, Palaeoclimatology, Palaeoecology* 231, 169–180.
- Mikolajewicz, U., 1998. Effect of meltwater input from the Antarctic ice sheet on the thermohaline circulation. *Annals of Glaciology* 27, 311–315.
- Monbeig-Andrieu, M., Cailleux, A., 1962. Grains éolisés dans les grès erratiques de Terre Adélie. *C.R. Soc. Géol. Fr.* 5, 151.
- Morgan, V.I., Wookey, C.W., Li, J., Ommen, T.D.V., Skinner, W., Fitzpatrick, M.F., 1997. Site information and initial results from deep ice drilling on Law Dome. *Journal of Glaciology* 43, 3–10.
- Naughton, F., Bourillet, J.F., Goñi, M.F.S., Turon, J.L., Jouanneau, J.M., 2007. Long-term and millennial-scale climate variability in northwestern France during the last 8850 years. *Holocene* 17, 939–953.
- Nielsen, S.H.H., Koç, N., Crosta, X., 2004. Holocene climate in the Atlantic sector of the Southern Ocean: Controlled by insolation or oceanic circulation? *Geology* 32, 317–320.
- Oerlemans, J., Nick, F.M., 2006. Modelling the advance-retreat cycle of a tidewater glacier with simple sediment dynamics. *Global and Planetary Change* 50, 148–160.
- Oppo, D.W., McManus, J.F., Cullen, J.L., 2003. Deepwater variability in the Holocene Epoch. *Nature* 422, 277–278.

- Periard, C., Petre, P., 1993. Some aspects of the climatology of Dumont d'Urville, Adélie Land, Antarctica. *International Journal of Climatology* 13 (3), 313–327.
- Porter, S.C., 1975. Equilibrium-line altitudes of late Quaternary glaciers in the Southern Alps, New Zealand. *Quaternary Research* 5, 27–47.
- Presti, M., De Santis, L., Busetti, M., Harris, P.T., 2003. Late Pleistocene and Holocene sedimentation on the George V Continental Shelf, East Antarctica. *Deep Sea Research Part II: Topical Studies in Oceanography* 50, 1441–1461.
- Rasmussen, T.L., Backstrom, D., Heinemeier, J., Klitgaard-Kristensen, D., Knutz, P.C., Kuijpers, A., Lassen, S., Thomsen, E., Troelstra, S.R., Van Weering, T.C.E., 2002. The Faroe–Shetland Gateway: Late Quaternary water mass exchange between the Nordic seas and the northeastern Atlantic. *Marine Geology* 188, 165–192.
- Renssen, H., Goosse, H., Fichefet, T., Massom–Delmotte, V.A., Koç, N., 2005a. Holocene climate evolution in the high-latitude Southern Hemisphere simulated by a coupled atmosphere–sea–ice–ocean–vegetation model. *The Holocene* 15, 951–964.
- Renssen, H., Goosse, H., Fichefet, T., Brovkin, V., Driesschaert, E., Wolk, F., 2005b. Simulating the Holocene climate evolution at northern high latitudes using a coupled atmosphere–sea ice–ocean–vegetation model. *Climate Dynamics* 24, 23–43.
- Richardson, G., Wadley, M.R., Heywood, K.J., Stevens, D.P., Banks, H.T., 2005. Short-term climate response to a freshwater pulse in the Southern Ocean. *Geophysical Research Letters* 32, 1–4.
- Rind, D., 2000. Relating paleoclimate data and past temperature gradients: Some suggestive rules. *Quaternary Science Reviews* 19, 381–390.
- Rintoul, S.R., 1998. On the origins and influence of Adélie Land bottom water. In: Jacobs, S.S., Weiss, R.F. (Eds.), *Ocean, Ice and Atmosphere: Interactions at the Antarctic Continental Margin*. Antarctic Research Series, vol. 75, pp. 151–171.
- Rintoul, S.R., Bullister, J.L., 1999. A late winter hydrographic section from Tasmania to Antarctica. *Deep Sea Research Part I. Oceanographic Research Papers* 46, 1417–1454.
- Roberts, D., McMinn, A., Cremer, H., Gore, D.B., Melles, M., 2004. The Holocene evolution and palaeosalinity history of Beall Lake, Windmill Islands (East Antarctica) using an expanded diatom-based weighted averaging model. *Palaeogeography, Palaeoclimatology, Palaeoecology* 208, 121–140.
- Rohling, E.J., Pälike, H., 2005. Centennial-scale climate cooling with a sudden cold event around 8200 years ago. *Nature* 434, 975–979.
- Sarnthein, M., Winn, K., Jung, S.J.A., Duplessy, J.-C., Labeyrie, L., Herlenkeuser, H., Ganssen, G., 1994. Changes in east Atlantic deepwater circulation over the last 30,000 years: Eight time slice reconstructions. *Paleoceanography* 9 (2), 209–267.
- Schmidt, S., 2006. Impact of Mediterranean Outflow Water on particle dynamics in intermediate waters of the North-East Atlantic, as revealed by 234Th and 228Th. *Marine Chemistry* 100, 289–298.
- Schmittner, A., 2003. Southern Ocean sea ice and radiocarbon ages of glacial bottom waters. *Earth and Planetary Science Letters* 213, 53–62.
- Schweitzer, P.N., 1995. Monthly Averaged Polar Sea Ice Concentration. U.S. Geological Survey Digital Data Series, Virginia.
- Shipp, S., Anderson, J., Domack, E., 1999. Late Pleistocene–Holocene retreat of the West Antarctic ice-sheet system in the Ross Sea: Part 1—Geophysical results. *Bulletin of the Geological Society of America* 111, 1486–1516.
- Sicre, M.A., Labeyrie, L., Ezat, U., Duprat, J., Turon, J.L., Schmidt, S., Michel, E., Mazaud, A., 2005. Mid-latitude Southern Indian Ocean response to Northern Hemisphere Heinrich events. *Earth and Planetary Science Letters* 240, 724–731.
- Solignac, S., de Vernal, A., Hillaire-Marcel, C., 2004. Holocene sea-surface conditions in the North Atlantic—contrasted trends and regimes in the western and eastern sectors (Labrador Sea vs. Iceland Basin). *Quaternary Science Reviews* 23, 319–334.
- Solomina, O., Haeblerli, W., Kull, C., Wiles, G., 2008. Historical and Holocene glacier–climate variations: General concepts and overview. *Global and Planetary Change* 60, 1–9.
- Stager, J.C., Mayewski, P.A., 1997. Abrupt Early to Mid-Holocene climatic transition registered at the equator and the poles. *Science* 276, 1834–1836.
- Stager, J.C., Cumming, B.F., Meeker, L.D., 2003. A 10,000-year high-resolution diatom record from Pilkington Bay, Lake Victoria, East Africa. *Quaternary Research* 59, 172–181.
- Steig, E.J., Morse, D.L., Waddington, E.D., Stuiver, M., Grootes, P.M., Mayewski, P.A., Twickler, M.S., Whitlows, S.L., 2000. Wisconsinan and Holocene climate history from an ice core at Taylor Dome, western Ross embayment, Antarctica. *Geografiska Annaler, Series A: Physical Geography* 82, 213–232.
- Stouffer, R.J., Seidov, D., Haupt, B.J., 2007. Climate response to external sources of freshwater: North Atlantic versus the Southern Ocean. *Journal of Climate* 20, 436–448.
- Stuiver, M., Reimer, P.J., Reimer, R.W., 2005. CALIB 5.0. [WWW program and documentation].
- Taylor, F., McMinn, A., 2002. Late Quaternary diatom assemblages from Prydz Bay, Eastern Antarctica. *Quaternary Research* 57, 151–161.
- van Beek, P., Reys, J.L., Paterne, M., Gersonde, R., van der Loeff, M.R., Kuhn, G., 2002. 226Ra in barite: Absolute dating of Holocene Southern Ocean sediments and reconstruction of sea-surface reservoir ages. *Geology* 30, 731–734.
- van Ommen, T.D., Morgan, V.I., Curran, M.A.J., 2004. Deglacial and Holocene changes in accumulation at Law Dome. *Annals of Glaciology* 39, 359–365.
- Veeh, H.H., McCorkle, D.C., Heggie, D.T., 2000. Glacial/interglacial variations of sedimentation on the West Australian continental margin: constraints from excess 230Th. *Marine Geology* 166, 11–30.
- Verkulich, S.R., Melles, M., Hubberten, H.-W., Pushina, Z.V., 2002. Holocene environmental changes and evolution of Figurnoye Lake in the southern Bunge Hills, East Antarctica. *Journal of Paleolimnology* 28, 253–267.
- Vimeux, F., Masson, V., Jouzel, J., Petit, J.R., Steig, E.J., Stievenard, M., Vaikmae, R., White, J.W.C., 2001. Holocene hydrological cycle changes in the Southern Hemisphere documented in East Antarctic deuterium excess records. *Climate Dynamics* 17, 503–513.
- Wagner, B., Melles, M., 2007. The heterogeneity of Holocene climatic and environmental history along the East Antarctic coastal regions. In: Cooper, A.K., Raymond, C.R. et al. (Eds.), *Antarctica: a keystone in a Changing World—Online Proceedings of the 10th ISAES, USGS Open-file Report 2007-1047, Extended Abstract 161*, 4 pp.
- Williams, G.D., Bindoff, N.L., 2003. Wintertime oceanography of the Adélie Depression. *Deep-Sea Research II* 50, 1373–1392.
- Yoon, H.I., Khim, B.K., Yoo, K.C., Bak, Y.S., Lee, J.I., 2007. Late glacial to Holocene climatic and oceanographic record of sediment facies from the South Scotia Sea off the northern Antarctic Peninsula. *Deep Sea Research Part II: Topical Studies in Oceanography* 54, 2367–2387.
- Zaragosi, S., Bourillet, J.-F., Eynaud, F., Toucanne, S., Denhard, B., Van Toer, A., Lanfumey, V., 2006. The impact of the last European deglaciation on the deep-sea turbidite systems of the Celtic-Armorian margin (Bay of Biscay). *Geo-Marine Letters* 26, 317–329.